

Role of Symmetry in Raman Spectroscopy of Unconventional Superconductors

T. P. Devereaux

Department of Physics
University of California, Davis, CA 95616

January 6, 2019

January 6, 2019

ABSTRACT

The role of symmetry of the inelastic light scattering amplitude, the superconducting energy gap, and the underlying Fermi surface manifold on the Raman spectra of unconventional superconductors is discussed in detail. Particular emphasis is placed on both single and bi-layer superconductors. It is found that the B_{1g} channel may be the most sensitive to doping due to the role of the Van Hove singularity. Lastly the effect of both disorder and spin fluctuations is considered. The theory imposes strong constraints on both the magnitude and symmetry of the energy gap for the bi-layer cuprates, indicating that a nearly identical energy gap of $d_{x^2-y^2}$ symmetry provides a best fit to the data.

Keywords: Raman scattering, unconventional superconductivity, bi-layer, spin fluctuations, impurities.

1 Introduction

In the recent few years Raman scattering has been proved to be a very powerful tool to study the anisotropy of the superconducting energy gap in high T_c superconductors. The rich information provided from experiments lies in the polarization dependence of the obtained spectra for small light energy transfers. The recent experiments carried out in different high T_c materials near optimal doping provide almost identical spectra showing very characteristic differences between the various polarization orientations.^{1,2,3} This polarization dependence, which is minimal in conventional superconductors, can be understood in unconventional superconductors primarily in terms of symmetry.

The light scattering amplitude can be given to lowest order in the vector potential as a sum of the three terms which correspond to direct photon scattering via electron-hole pair production and via photon absorption and emission through an intermediate state. In the limit of zero momentum photon transfer this vertex can be written

in the form^{4,5}

$$\gamma(\mathbf{k}; \omega_I, \omega_S) = \mathbf{e}^I \cdot \mathbf{e}^S + m^{-1} \sum_{\nu} \left\{ \frac{(\mathbf{k} | \mathbf{k} \cdot \mathbf{e}^S | \nu \mathbf{k})(\nu \mathbf{k} | \mathbf{k} \cdot \mathbf{e}^I | \mathbf{k})}{\epsilon_{\mathbf{k}} - \epsilon_{\nu, \mathbf{k}} + \omega_I} + \frac{(\mathbf{k} | \mathbf{k} \cdot \mathbf{e}^I | \nu \mathbf{k})(\nu \mathbf{k} | \mathbf{k} \cdot \mathbf{e}^S | \mathbf{k})}{\epsilon_{\mathbf{k}} - \epsilon_{\nu, \mathbf{k}} - \omega_S} \right\}, \quad (1)$$

where m is the electron mass, ν stands for the intermediate state $|\nu \mathbf{k}\rangle$ of the electron excited out of the conduction band $|\mathbf{k}\rangle$ with dispersion $\epsilon_{\mathbf{k}}$, $\omega_{I,S}$ and $\mathbf{e}^{I,S}$ are the incident and scattered photon energies and polarizations, respectively.

According to Abrikosov and Genkin if the energy of the incident and scattered frequencies are negligible compared to the relevant electronic energy scale, γ can be expressed in terms of the curvature of the conduction band and the incident and scattered photon polarization vectors $\mathbf{e}^{I,S}$ as⁵

$$\lim_{\omega_I, \omega_S \rightarrow 0} \gamma(\mathbf{k}; \omega_I, \omega_S) = \sum_{\mu, \nu} e_{\mu}^I \frac{\partial^2 \epsilon(\mathbf{k})}{\partial k_{\mu} \partial k_{\nu}} e_{\nu}^S, \quad (2)$$

where terms of the order of $1 - \omega_S/\omega_I$ are dropped. This effective mass approximation has been extensively used to calculate the Raman spectra in unconventional superconductors.

This approximation holds only for small energy transfers *and* provided that the bands are not nearly degenerate. Thus one might question the appropriateness of this approximation for the cuprates given that typical incoming laser frequencies are on the order of 2 eV - certainly on the order of the relevant electronic energy scale for a single band. For the case of two bands near or crossing the Fermi level, the effective mass approximation is even more questionable. Since in the bi-layer superconductors Bi 2:2:1:2 and Y 1:2:3 the band splitting of the even and odd bands is on the order of tens of meVs, the approximation misses large terms corresponding to interband transitions at relatively small energies. Detailed knowledge of the magnitude of the scattering amplitude in this case requires knowledge of the wave functions of the two states, which has currently not been investigated. Thereby, use of the effective mass approximation is uncontrolled in many band systems and comparisons to experiment intensities must be viewed with caution.

An alternative approach is based on the experimental observation that the spectra near optimal doping for a wide range of cuprate materials depends only mildly on the incoming laser frequency. Since the polarization orientations transform as various elements of the point group of the crystal, one can use symmetry to classify the scattering amplitude, viz.,

$$\gamma(\mathbf{k}; \omega_I, \omega_S) = \sum_L \gamma_L(\omega_I, \omega_S) \Phi_L(\mathbf{k}), \quad (3)$$

where $\Phi_L(\mathbf{k})$ are either Brillouin zone (B.Z.H., orthogonal over the entire Brillouin zone) or Fermi surface (F.S.H., orthogonal on the Fermi surface only) harmonics which transform according to point group transformations of the crystal.⁶ Representing the magnitude but not the \mathbf{k} -dependence of both intra- and interband scattering, the prefactors can be approximated to be frequency independent and taken as model constants to fit absolute intensities. Thus we have simplified the many-band problem in terms of symmetry components which can be related to charge degrees of freedom on portions of the Fermi sheets. While sacrificing information pertaining to overall intensities, we have gained the ability to probe and compare excitations on different regions of the Fermi surface based solely on symmetry classifications. This can be illustrated by considering the various experimentally accessible polarization orientations.

In the following we confine ourselves to tetragonal systems with in-plane lattice constant a , and for the moment consider uncoupled planes which can be modelled by the following band structure:

$$\epsilon(\mathbf{k}) = -2t[\cos(k_x a) + \cos(k_y a)] + 4t' \cos(k_x a) \cos(k_y a) - 2t''[\cos(2k_x a) + \cos(2k_y a)] - \mu. \quad (4)$$

We will consider coupling between the planes in the second part of the following section. Using an x, y coordinate system locked to the CuO_2 planes, incident and scattered light polarizations aligned along $\hat{x} + \hat{y}$, $\hat{x} - \hat{y}$ for example transform according to B_{1g} symmetry, and thus

$$\Phi_{B_{1g}}(\mathbf{k}) = \cos(k_x a) - \cos(k_y a) + \dots, \quad (5)$$

where ... are higher order B.Z.H. Likewise, $\mathbf{e}^{I,S}$ aligned along \hat{x}, \hat{y} transforms as B_{2g} :

$$\Phi_{B_{2g}}(\mathbf{k}) = \sin(k_x a) \sin(k_y a) + \dots \quad (6)$$

The A_{1g} basis function is

$$\Phi_{A_{1g}}(\mathbf{k}) = a_0 + a_2[\cos(k_x a) + \cos(k_y a)] + a_4 \cos(k_x a) \cos(k_y a) + a_6[\cos(2k_x a) + \cos(2k_y a)] + \dots, \quad (7)$$

where the expansion parameters a_i determined via a fitting procedure with experiment.⁷ The A_{1g} response is not directly accessible from experiments and must be obtained by subtracting several combinations of the response for various polarization orientations.

By considering the \mathbf{k} -dependence of the basis functions, it is clear that the B_{1g} part of the spectra essentially probes light scattering events along the k_x or k_y axes, B_{2g} probes the diagonals, and A_{1g} is more of an average over the entire Brillouin zone. It is in this manner that information about the momentum dependence of the superconducting energy gap can be usefully extracted from the data.¹ That information lies in two important aspects: the low frequency power-law behavior of the spectra and the positions of the low energy peaks.

2 Raman Response for Unconventional Superconductors

The spectra can be obtained via the two-particle Raman correlation function and is derivable either via Green's function or kinetic equation approach. In the following sections, the response is calculated for the case of a single band model and a superconducting bi-layer.

2.1 Single Band

For a single band crossing the Fermi surface, the response can be written in the "Pair Approximation"⁸ in terms of the Tsuneto function λ as⁹

$$\chi_{\gamma,\gamma}(\mathbf{q} = 0, i\omega) = \sum_{\mathbf{k}} \gamma(\mathbf{k}; i\omega_I, i\omega_S)^2 \lambda(\mathbf{k}, i\omega); \quad \lambda(\mathbf{k}, i\omega) = \frac{\Delta(\mathbf{k})^2}{E(\mathbf{k})^2} \tanh \left[\frac{E(\mathbf{k})}{2T} \right] \left[\frac{1}{2E(\mathbf{k}) + i\omega} + \frac{1}{2E(\mathbf{k}) - i\omega} \right]. \quad (8)$$

Here $E(\mathbf{k})^2 = \epsilon(\mathbf{k})^2 + \Delta(\mathbf{k})^2$ and we have set $k_B = \hbar = 1$. The light scattering cross section is obtained by taking the imaginary part via analytic continuation. We have neglected vertex corrections of the pairing interactions which while responsible for maintaining gauge invariance and producing collective modes, can be shown to have only a limited effect on the spectra at low energies for d -wave superconductors.⁹ The long-range part of Coulomb interaction is not included at this stage, but will be shown to be very important for the A_{1g} response.

Eq. (8) and approximations to it have been evaluated previously for various forms of the energy gap $\Delta(\mathbf{k})$. The response has been evaluated using a simpler tight binding parametrization of the energy band dispersion by (i) restricting the sum to the Fermi surface using a weak coupling energy gap,^{2,9} and (ii) performing the \mathbf{k} -sums directly while using a phenomenological spin fluctuation mediated energy gap.¹⁰ These are improvements on the original consideration which approximated the Fermi surface to be nearly cylindrical.¹

In this section the $T \ll T_c$ Raman response for a single CuO layer is obtained by evaluating the \mathbf{k} -sums directly in order to capture the charge dynamics over the entire Brillouin zone, and in particular the role of the Van Hove singularities can be examined. We focus attention on La 2:1:4¹¹ and Y 1:2:3¹² as representative calculations.

The B_{1g} and B_{2g} responses are plotted in Fig. 1 using an energy gap of $d_{x^2-y^2}$ symmetry. In both cases, the B_{1g} response for low frequencies varies as ω^3 while the B_{2g} varies linearly with ω . This can be shown to be

generally true for these channels for any number of higher harmonics used, and results from a consideration of the density of states (DOS), which varies linearly with energy due to the nodes, and the behavior of the Raman vertex γ near the gap nodes. Since the B_{2g} vertex is finite near the nodes, the DOS determines the low frequency behavior. However, the gap and the vertex vanish at the same place for the B_{1g} channel, which in turn leads to the cubic behavior. This delicate interplay of vertex and energy gap can thus provide a unique determination of the nodal gap behavior.

Moreover, additional information lies in the peaks of the spectra. A smooth peak is seen for B_{2g} and a double-peak is obtained for B_{1g} . The lower peak is due to the energy gap while the other comes from the Van Hove singularity. The peak of the spectra due to superconductivity in both cases is higher for the B_{1g} channel ($\omega_{peak} = 2\Delta_{max}$) than for B_{2g} , ($\omega_{peak} \sim 1.7\Delta_{max}$) since the gap maxima are located at the same part of the Fermi surface where the B_{1g} basis function is largest, and where the B_{2g} basis function vanishes. This is generally true regardless of Fermi surface shape, although the relative positions of the peaks can be affected slightly by changing the underlying manifold (see Fig 2a and 2b and Refs.^{1,2,9}). The shape of the spectra can also be mildly modified by considering higher harmonics of the energy gap¹⁰ and/or by including final-state interactions⁹ or impurity scattering.¹³ Apart from the last case, the power-law behaviors at low frequencies are unaffected and therefore their observation is a robust check on the symmetry of the energy gap.

The Van Hove peak only shows up in the B_{1g} channel since the B_{2g} channel assigns no weight to the location of the Van Hove points. The Van Hove peak lies at a higher energy determined by its location off the Fermi surface and the value of the energy gap there. There are indications that a double-peak feature has been seen in underdoped Y 1:2:3 with a $T_c = 60K$.¹⁴ As the Van Hove moves further away from the Fermi surface for example with doping, the peak shifts to higher frequencies and has a smaller residue. Inelastic scattering at higher energies will also act to smear out this feature and thus a single smeared and perhaps asymmetric peak would be seen if the Van Hove lies quite near the Fermi surface, and could in principle move the B_{1g} peak slightly above $2\Delta_{max}$. This may be reflected in the experiments of Ref.¹⁵ which saw a sensitivity of the B_{1g} peak position to doping.

We now turn to the A_{1g} channel. Here the long-range Coulomb screening plays a very important role. Namely, those parts of the spectra which are coupled to the Coulomb fields are screened and do not appear in the limit of small momentum transfer $q \rightarrow 0$, as is always the case. The long-range Coulomb forces play an important role if there is charge transfer between unit cells at large distances. Thus only the charges produced by charge transfers inside the unit cell determine the measurable spectra. This transfer is between the different atoms in the cell or the redistribution of the electrons between different parts of the Fermi surface or between different Fermi surfaces. In this way, only the A_{1g} part of the spectra can be coupled to the Coulomb forces since for the case of B_{1g} and B_{2g} channels, the Coulomb corrections vanish due to symmetry.

Including the long-range Coulomb interaction, the A_{1g} response can be written as^{4,9}

$$\chi_{\gamma,\gamma}^{A_{1g}}(i\omega) = \chi_{\gamma,\gamma}(i\omega) - \frac{[\chi_{1,\gamma}(i\omega)]^2}{\chi_{1,1}(i\omega)}, \quad (9)$$

where $\chi_{a,b}$ is given by Eq. (8) with vertices a, b replacing γ . Writing the A_{1g} vertex as $\gamma(\mathbf{k}) = \langle \gamma(\mathbf{k}) \rangle + \delta\gamma(\mathbf{k})$, where $\langle \gamma(\mathbf{k}) \rangle$ is the average vertex over the Brillouin zone, and inserting into Eq. (9) one finds that indeed the long-range Coulomb interaction completely screens the constant contribution to the vertex, or the intercell charge fluctuation contribution, and thus only the intracell fluctuations can scatter light in the limit of $q = 0$.

In Fig. 2 we show a calculation of the unscreened and screened A_{1g} response for a $d_{x^2-y^2}$ paired superconductor for the Y 1:2:3 parameters. We have chosen the coefficients a_i in Eq. (7) using the effective mass approximation,⁷ but we note that the results do not depend dramatically on the choice of coefficient sets. By again considering the nature of the nodal structure of the energy gap, since the A_{1g} response measures a weighted average of charge fluctuations around the Fermi surface, it can be shown that the low energy part of the A_{1g} response must vary with energy in the same way as the DOS.

The screened and unscreened responses at higher energies are very different. For the unscreened response, two

peaks arise corresponding to the singular contribution of pair breaking along the axes and the Van Hove contribution as in the B_{1g} channel. Screening completely reorganizes the spectra to remove both peak contributions, replacing them with a much smoother peak at lower energies. This is due to the screening function (2nd part of Eq. (9)) which also contains peaks at $2\Delta_{max}$ due to the weighting along the k_x and k_y axes, and the Van Hove. These peaks cancel the unscreened peaks and creates a near peak lying at slightly greater than Δ_{max} , as seen in Fig. 2.

In this manner, similar symmetry considerations can be made for various types of energy gaps. The Raman spectra calculated for various energy gaps is summarized in Table 1 and compared to the low energy DOS $N(\omega)$. The dominant contribution to the Raman lineshape is due to the location and behavior of the energy gap near both the nodes and the maxima. Subsequently, different energy gaps produce different line shapes as summarized in Table 1. Here it is important to note that the cubic rise of the spectra in any channel requires that both the vertex and the energy gap have the same behavior near the nodes. In tetragonal systems, this requires the presence of a $d_{x^2-y^2}$ energy gap. By considering small orthorhombic distortions, the A_{1g} and B_{1g} channels become mixed and therefore a linear rise with frequency could be obtained at low energies in a region determined by the amount of symmetry breaking. Since experimentally the low frequency part of the B_{1g} spectra rises cubically in the most tetragonal systems, while in Y 1:2:3 the spectra has a small linear part, this strongly suggests the likelihood of a $d_{x^2-y^2}$ pair state for these systems. Exploration of the low frequency part of the spectra could put stringent constraints on other pair-state candidates.

2.2 Bi-Layer

The above consideration must be reformulated for the case of two or more bands crossing the Fermi level.¹⁶ In particular, the role of screening is more subtle in this case. The above arguments on the role of Coulomb screening is based on the assumption that only one Fermi surface is relevant, which is very reasonable for materials with a single CuO_2 plane in the unit cell. Recently Krantz and Cardona¹⁷ have raised the relevant question how a double-sheeted Fermi surface, as occurs in materials with more than one CuO_2 planes in the unit cell, changes the above argument. In particular, the main question is whether or not in the bi-layer compound a singularity can occur at $2\Delta_{max}$ in the A_{1g} symmetry, similar to the one which occurs in the B_{1g} case, due to the avoidance of screening.

Considering the electronic density, the singular regions of the Fermi surface are near the k_x and k_y axes, respectively. The two layers double the number of these regions. In the case of B_{1g} symmetry the charge transfer changes sign going from one region to the other. In contrast, in the case of A_{1g} symmetry, each region has the same phase on a particular Fermi surface. Therefore, in the case of the single layer material, considering the singular part, the charge transfer is only between different cells, which is screened. In the bi-layer case, the A_{1g} symmetry allows a charge transfer between the two layers of both the same and opposite sign on each Fermi surface. While the addition of the two charge density distributions is still an intercell charge transfer and is thus screened, if the bands are non-degenerate then the difference of the two distributions can survive screening and could thus in principle give a singular contribution at $2\Delta_{max}$.

It is straightforward repeat the previous calculations for the two band model. The calculation proceeds by first considering charge density-like fluctuations on each CuO_2 plane and allow for charge to be transferred between the planes due to an interplane coupling matrix element t_\perp through which electrons can hop from one plane to the other directly or through an intermediate state such as the chains or Y atoms. Details of the calculation can be found in Ref.¹⁶ Diagonalizing the Hamiltonian by introducing even and odd combinations of electron operators in the two planes, we arrive at the following compact expression for the cross section:

$$\chi''(\omega) = \sum_{\mathbf{k}, \pm} [\gamma(\mathbf{k}) \pm \gamma_{1,2}(\mathbf{k})]^2 \lambda''_{\pm}(\mathbf{k}, \omega) - \left\{ \frac{\left(\sum_{\mathbf{k}, \pm} [\gamma(\mathbf{k}) \pm \gamma_{1,2}(\mathbf{k})] \lambda_{\pm}(\mathbf{k}, i\omega) \right)^2}{\sum_{\mathbf{k}, \pm} \lambda_{\pm}(\mathbf{k}, i\omega)} \right\}'' . \quad (10)$$

Here λ_{\pm} is the Tsuneto function for the bonding (anti-bonding) band, $\epsilon_{\pm}(\mathbf{k}) = \epsilon(\mathbf{k}) \mp t_{\perp}(\mathbf{k})$, and the vertices are given by

$$\gamma(\mathbf{k}) = \gamma_{1,1}(\mathbf{k}) + \gamma_{2,2}(\mathbf{k}) = \frac{1}{2}[\gamma_{+}(\mathbf{k}) + \gamma_{-}(\mathbf{k})]; \quad \gamma_{1,2}(\mathbf{k}) = \frac{1}{2}[\gamma_{+}(\mathbf{k}) - \gamma_{-}(\mathbf{k})]. \quad (11)$$

This corresponds to a diagonal contribution which allows light to be scattered by density-like fluctuations on either plane 1 ($\gamma_{1,1}$) or plane 2 ($\gamma_{2,2}$) and an off-diagonal term ($\gamma_{1,2}$) which allows light scattering on both planes simultaneously. Since in the limit of $\mathbf{q} \rightarrow 0$ the long-range intercell fluctuations are screened, only the intracell fluctuations remain. Therefore only charge transfer fluctuations between the atoms in the plane and outside the plane (e.g., Y and the chains), and between the planes can effectively cause light scattering. Since experimentally the interlayer coupling is small, the resulting vertex $\gamma_{1,2}$ must be smaller than the + combination, labelled as γ .

Rearranging terms, we can cast the result in terms of an addition of the result for each single band plus a mixing term:

$$\chi''(\omega) = \chi''_{+}(\omega) + \chi''_{-}(\omega) + \Delta\chi''(\omega), \quad (12)$$

where

$$\chi''_{\pm}(\omega) = \sum_{\mathbf{k}} \gamma_{\pm}^2(\mathbf{k}) \lambda_{\pm}''(\mathbf{k}, \omega) - \left\{ \frac{(\sum_{\mathbf{k}} \gamma_{\pm}(\mathbf{k}) \lambda_{\pm}(\mathbf{k}, i\omega))^2}{\sum_{\mathbf{k}} \lambda_{\pm}(\mathbf{k}, i\omega)} \right\}''; \quad (13)$$

$$\Delta\chi''(\omega) = \left\{ \frac{(\sum_{\mathbf{k}} \lambda_{+}(\mathbf{k}, i\omega)) (\sum_{\mathbf{k}} \lambda_{-}(\mathbf{k}, i\omega))}{\sum_{\mathbf{k}, \pm} \lambda_{\pm}(\mathbf{k}, i\omega)} \left[\frac{\sum_{\mathbf{k}} \gamma_{+}(\mathbf{k}) \lambda_{+}(\mathbf{k}, i\omega)}{\sum_{\mathbf{k}} \lambda_{+}(\mathbf{k}, i\omega)} - \frac{\sum_{\mathbf{k}} \gamma_{-}(\mathbf{k}) \lambda_{-}(\mathbf{k}, i\omega)}{\sum_{\mathbf{k}} \lambda_{-}(\mathbf{k}, i\omega)} \right]^2 \right\}'' . \quad (14)$$

Eqs. (12-14) shows that the total response can be considered as a sum of the single band contributions in addition to a mixing term which corresponds to odd combinations of fluctuations on the bands simultaneously. In order to discern the features of the mixing term, it is useful to write $\gamma_{\pm}(\mathbf{k}) = \gamma_{\pm}^0 + \Delta\gamma_{\pm}(\mathbf{k})$, where the average of $\Delta\gamma(\mathbf{k})$ around the Fermi surface vanishes.

Then it useful to consider the following cases:

(1) If the layers are uncoupled, then $\gamma_{+}(\mathbf{k}) = \gamma_{-}(\mathbf{k})$ and the mixing term vanishes: $\Delta\chi''(\omega) = 0$.

(2) If the scattering in the A_{1g} symmetry channel γ is independent of \mathbf{k} (scattering on real charge), then $\Delta\chi \sim (\gamma_{+}^0 - \gamma_{-}^0)^2 \sim \gamma_{1,2}^2$. This means that the light scattering induces an interlayer charge transfer. However, it can be seen by the first term on the r.h.s. of Eq. (14) that in order for a divergence to occur above the peak for the single band result, then the energy gaps on each band must be identical. Otherwise, the divergences in the numerator and denominator cancel each other and a smoothly varying response is obtained.

(3) Considering when the light induces charge transfers on different parts of the Fermi surfaces, $\Delta\gamma_{\pm}(\mathbf{k})$ must be included and includes different symmetry channels depending on the orientation of the incident and scattered light polarizations. A_{1g} symmetry reflects the approximate tetragonal symmetry of the CuO_2 planes, while the part of γ showing symmetries different than A_{1g} (e.g., B_{1g} , B_{2g} and E_g) changes sign when symmetry transformations are applied. The Tsuneto function depends only on the energy gap squared, and thus all the sums in Eq. (14) are zero except for the A_{1g} component of $\Delta\gamma_{\pm}(\mathbf{k})$. For tetragonal materials, this means that the B_{1g} , B_{2g} , and E_g channels do not have a mixing term and therefore the total response for these channels is simply the additive contributions from each single band. The mixing term only contributes to the A_{1g} channel, the strength of which is roughly determined by the interlayer coupling.

These points can be easily illustrated by considering a bi-layer superconductor with energy gaps $\Delta_{\pm}(\mathbf{k}) = \Delta_{\pm}[\cos(k_x a) - \cos(k_y a)]$ on the two bands. For the interlayer coupling t_{\perp} , we follow Ref.¹² and define

$$t_{\perp}(\mathbf{k}) = t_{\perp}[\cos(k_x a) - \cos(k_y a)]^2, \quad (15)$$

with $t_{\perp}/t = 0.2$. In the absence of inter-layer coupling the chemical potential is chosen so that $\langle n \rangle = 0.8$. Lastly, we consider the case where $\Delta_{\pm} = 15$ meV for both bands.

The resulting spectra for the bonding and anti-bonding bands, as well as the mixing term for A_{1g} are shown in Fig. 3. Here again we have used the effective mass approximation for the expansion parameters of Eq. 7 for illustration.⁷ Considering the B_{1g} and B_{2g} channels, which are simply additive, it can be inferred from experimental result which shows only one peak in these channels that either the energy gap is nearly identical both in symmetry and magnitude or alternatively that the Raman response is given predominantly by one band. Otherwise two distinct peaks would appear (if gaps have different symmetry and/or magnitude) and identical power-law behavior for each channel would be seen (if the gaps were of different symmetry but same magnitude).¹⁸ Since the band splitting is relatively small in Y 1:2:3 and even smaller in Bi 2:2:1:2, the second possibility in our opinion is unlikely. Therefore, the energy gap on each band must be similar on energy scales determined by the amount of inelastic scattering which would smear a double-peak feature. Again we note that the sharp nature of the B_{1g} peak would imply that its position and shape would be most sensitive to the location of the Van Hove points for each band and the maximal value of the energy gaps.^{14,15}

Due to the small bi-layer splitting the mixing term for A_{1g} is small, as shown in Fig. (3). A very small peak at roughly $2\Delta_{max}$ (not divergent) is seen due to the odd combination of interlayer charge transfer, as suggested by Krantz and Cardona but is strongly suppressed. Since adding electron correlations suppresses the bi-layer splitting even further¹⁹ the mixing term is only of minor importance and the resulting spectra can be well approximated as the sum of the contributions from the two individual bands. In this way, a consistent picture can emerge since experimentally the electronic Raman spectra do not differ substantially in the bi-layer or single-layer materials.^{1,2,3}

3 Impurity and Spin Fluctuation Scattering

The previous considerations were limited to the case of clean superconductors in which light scattering only occurs via breaking of Cooper pairs. Since the limit of $\mathbf{q} \rightarrow \mathbf{0}$ was taken, as a consequence no scattering remains above T_c due to phase space constraints. Impurity and/or spin fluctuation scattering must therefore be taken into account in order to attempt to model the full spectra for a wider range of temperatures and frequencies. In closing, this section is devoted to including such scattering processes. The following discussion is mostly qualitative in nature. An earlier account of this work is provided in Ref.¹³

Isotropic impurity scattering can be easily incorporated using a T-matrix approach. This simplified approach [recent studies have shown that impurity scattering in a strongly correlated material can have a non-trivial k -dependence²¹] does not mix symmetry channels and therefore previous considerations can be applied. The scattering is then characterized by the phase shift δ , $c = \cot(\delta)$, and by the impurity concentration n_i , $\Gamma = n_i/\pi N_F$. Since we have seen that the shape of the Fermi surface has little effect on the low energy part of the cross section, we for simplicity take an infinite band and a nearly cylindrical Fermi surface [see Ref.⁹ for details]. Here we also consider only unitary scattering $c = 0$, and small impurity concentrations $\Gamma/\Delta_{max} = 0.01$. Other choices for the parameters are considered in a forthcoming publication.²⁰ While certainly a simplification of real systems, the salient features can be explored with some generality.

In order to incorporate spin fluctuation scattering, we follow the work of Ref.,²² who considered spin fluctuation scattering in a $d_{x^2-y^2}$ superconductor in the context of the infrared conductivity using a 2-D Hubbard model. There spin fluctuation scattering was incorporated in the imaginary part of the self energy while vertex corrections and the real part of the self energy were neglected. We follow the same approach here and use their interpolation result for the frequency dependent inelastic scattering rate, which was found at low temperatures to vary as ω^3 for frequencies below three times the maximum gap energy and then linearly thereafter:

$$\Gamma_{s.f}(\omega, T \ll T_c)/3\Delta_{max} = 0.7 \begin{cases} (\omega/3\Delta_{max})^3 & \text{for } \omega < 3\Delta_{max}, \\ \omega/3\Delta_{max} & \text{otherwise} \end{cases}, \quad (16)$$

which was obtained for $T = 0.1T_c$, $\langle n \rangle = 0.85$, $U = 2$ in a model with only nearest neighbor hopping. The scattering rate is approximated to be isotropic.

The additional scattering mechanisms modify the spectra in two important regards - the low frequency behavior, caused by impurity scattering, and the high frequency behavior caused by spin fluctuation scattering. This is shown in Fig. (4) for the B_{1g} and B_{2g} channels.

The impurity modifications on the density of states is reflected in the low frequency part of the spectra. Here the foot in the density of states causes the low frequency part of the spectra in each channel to rise linearly in frequency as it does in the normal state. This holds for the B_{1g} channel as well, where a crossover is seen at a frequency $\omega^* \sim \sqrt{\Gamma \Delta_{max}}$ which separates linear behavior below and cubic behavior above as seen in Fig. 4. This is the opposite of what one would expect if the energy gap were of anisotropic s -wave symmetry, since there spectral weight would be shifted to *higher* frequencies due to an opening of a gap.^{23,13} The only changes at higher frequencies comes from a smearing of the singularities at twice the gap edge.

Spin fluctuation scattering is relatively inoperative at low frequencies and thus does not produce any noticeable effects. However, the approximately linear in frequency behavior at large frequencies, as well as the value of the scattering rate at twice the gap edge modify the spectra at larger frequency shifts. The scattering at twice the gap edge effectively smears out any singularities due to the energy gap (or to the Van Hove). Further, a flat featureless background at larger frequencies is obtained. Similar results have been obtained by Jiang and Carbotte using a different model.²⁴

4 Conclusions

We have seen that electronic Raman scattering contains a wealth of information concerning the nature of superconductivity in unconventional superconductors which can be extracted from symmetry considerations alone.²⁶ When applied to the experimental data for *optimally* doped cuprate materials, good agreement can be obtained for $d_{x^2-y^2}$ pairing in single band materials, and nearly identical gaps of $d_{x^2-y^2}$ symmetry for bi-layer systems. The analysis is based on the prominent behavior of the spectra at low frequencies and the approximate position of the maxima for each channel.

However, further work is needed in order to understand the properties of the Raman spectra *away* from optimal doping.^{3,14,15,25} It is suggested that the B_{1g} peak may be the most sensitive to doping due to the role of the Van Hove singularity. However in order to understand the effects of doping in more detail, a particular model of superconductivity is needed, as is a more sophisticated approach for handling the spin degrees of freedom.

5 Acknowledgements

This work in part is done in collaboration with Drs. D. Einzel, A. Virosztek, and A. Zawadowski, and was supported by NSF Grant No. DMR 95-28535.

6 REFERENCES

- [1] T. P. Devereaux *et al.*, Phys. Rev. Lett. **72**, 396 (1994).
- [2] X. K. Chen *et al.*, Phys. Rev. Lett. **73**, 3290 (1994); Journ. of Supercond. **8**, 495 (1995).

- [3] S. L. Cooper *et al.*, Phys. Rev. B **37**, 5920 (1988); R. Hackl *et al.*, *ibid* **38**, 7133 (1988); S. L. Cooper *et al.*, *ibid*, 11934 (1988); T. Staufner *et al.*, Phys. Rev. Lett. **68**, 1069 (1992); R. Nemetschek *et al.*, Phys. Rev. B **47**, 3450 (1993); X. K. Chen *et al.*, *ibid*, 10530 (1993); A. Hoffmann *et al.*, Physica C **235-240**, 1897 (1994); C. Kendziora *et al.*, Phys. Rev. B **52**, 9867 (1995), and references therein.
- [4] M. V. Klein and S. B. Dierker, Phys. Rev. B **29**, 4976 (1984).
- [5] A. A. Abrikosov and V. M. Genkin, Zh. Eksp. Teor. Fiz. **40**, 842 (1973) [Sov. Phys. JETP **38**, 417 (1974)].
- [6] P. Allen, Phys. Rev. B **13**, 1416 (1976).
- [7] In the effective mass approximation Eq. (7) yields $a_0 = 0$, $a_2 = 2t$, $a_4 = -4t'$, and $a_6 = 2t''$.
- [8] R. E. Prange, Phys. Rev. **129**, 2495 (1963).
- [9] T. P. Devereaux and D. Einzel, Phys. Rev. B **51**, 16336 (1995); Journ. of Supercond. **8**, 421 (1995).
- [10] D. Branch and J. P. Carbotte, Phys. Rev. B **52**, 603 (1995); D. Branch, Master's Thesis (unpublished).
- [11] Q. Si *et al.*, Phys. Rev. B **47**, 9055 (1993).
- [12] G. Blumberg *et al.*, Phys. Rev. B **52**, 15741 (1995); O. K. Andersen *et al.*, Phys. Rev. B **49**, 4145 (1993); to appear in Journ. of Supercond.; R. J. Radtke *et al.*, preprint.
- [13] T. P. Devereaux, Phys. Rev. Lett. **74**, 4313 (1995).
- [14] F. Slakey *et al.*, Phys. Rev. B **42**, 2643 (1990).
- [15] X. K. Chen *et al.*, Phys. Rev. B **48**, 10530 (1993).
- [16] T. P. Devereaux, A. Virosztek, and A. Zawadowski, preprint.
- [17] M. C. Krantz and M. Cardona, Phys. Rev. Lett. **72**, 3290 (1994); Journ. of Low Temp. Phys. **99**, 205 (1995); T. P. Devereaux *et al.*, Phys. Rev. Lett. **72**, 3291 (1994).
- [18] The power-law behavior would not be changed if one of the gaps was the same magnitude as the other but completely isotropic *s*-wave. However, then all channels would show a sharply defined peak at $2\Delta_{max}$. This is in disagreement with experiment and appears to be unlikely.
- [19] A. I. Liechtenstein *et al.*, preprint; H. Ding *et al.*, preprint, and references therein.
- [20] T. P. Devereaux, to be published in Int. Journ. of Mod. Phys. B.
- [21] T. Xiang *et al.*, Phys. Rev. B **51**, 11721 (1995); D. Poilblanc *et al.*, Phys. Rev. Lett. **72**, 884 (1994).
- [22] S. M. Quinlan, P. J. Hirschfeld, and D. J. Scalapino, preprint.
- [23] L. S. Borkowski and P. J. Hirschfeld, Phys. Rev. B **49**, 15404 (1994), and references therein.
- [24] C. Jiang and J. P. Carbotte, Sol. State Commun. **95**, 643 (1995).
- [25] R. Hackl, J. C. Irwin and M. V. Klein, private communication.
- [26] Similar considerations can be applied to the optically active phonon lineshapes below T_c (see T. P. Devereaux *et al.*, Phys. Rev. B **51**, 505 (1995), and references therein).

TABLE I

Summary of Raman response for various pair state candidates for clean, tetragonal superconductors.*

$\Delta(\mathbf{k})$	$N(\omega \rightarrow 0)$	B_{1g}		B_{2g}		A_{1g}	
		$\chi''(\omega \rightarrow 0)$	$\frac{\omega_{peak}}{\Delta_{max}}$	$\chi''(\omega \rightarrow 0)$	$\frac{\omega_{peak}}{\Delta_{max}}$	$\chi''(\omega \rightarrow 0)$	$\frac{\omega_{peak}}{\Delta_{max}}$
isotropic s -wave	$\Theta(\omega - \Delta)$	$\Theta(\omega - 2\Delta)$	2	$\Theta(\omega - 2\Delta)$	2	$\Theta(\omega - 2\Delta)$	2
$d_{x^2-y^2}$	ω	ω^3	2	ω	~ 1.7	ω	~ 1.2
$s + id_{x^2-y^2}$	$\Theta(\omega - \Delta_s)$	$\Theta(\omega - 2\Delta_s)$	2	$\Theta(\omega - 2\Delta_s)$	$2\Delta_s/\Delta_d$	$\Theta(\omega - 2\Delta_s)$	$2\Delta_s/\Delta_d$
d_{xy}	ω	ω	~ 1.7	ω^3	2	ω	~ 1.2
$(d_{x^2-y^2})^m$	$\omega^{1/m}$	$\omega^{3/m}$	2	$\omega^{1/m}$	< 1.7	$\omega^{1/m}$	≤ 1.2
g -wave [†] $\sim \cos(k_x a) \cos(k_y a)$	ω	ω	2	ω	0.6	ω	0.6
extended s -wave ^{††} $\sim \cos(k_x a) + \cos(k_y a)$	ω	ω	~ 1.7	ω	2	ω	~ 1.2
experimental results for optimal doping	ω	ω^3	2	ω	1.5 \sim 1.8	ω	1.0 \sim 1.2

* Here phase is undetermined and thus $|d_{x^2-y^2}|$ would yield the same as $d_{x^2-y^2}$. Moreover, orthorhombic distortions will mix B_{1g} and A_{1g} channels.

[†] Parameters chosen to split node at 45° into two modes at $45^\circ \pm 5^\circ$ and a subsidiary maximum equal to 20 percent of gap maxima.

^{††} Parameters chosen such that $\langle n \rangle = 0.8$.

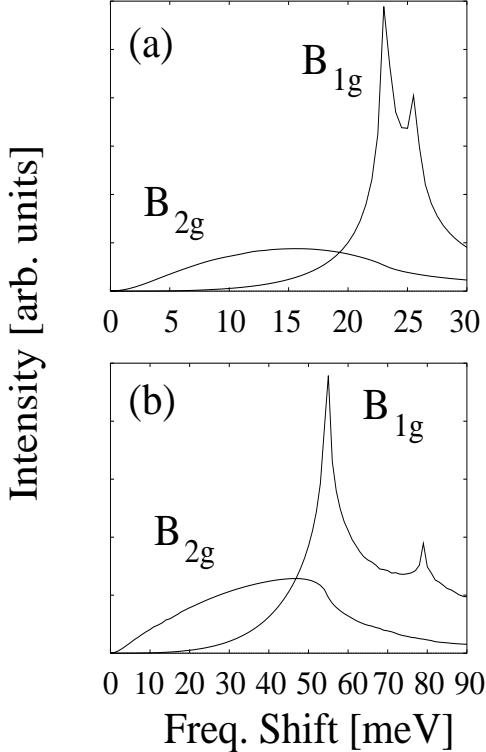


Figure 1: B_{1g} and B_{2g} Raman responses for a single band plotted for parameters sets for (a) La 2:1:4 and (b) Y 1:2:3. Here a filling $\langle n \rangle = 0.8$ and $t = 100$ meV, and $\Delta(k) = \Delta_0[\cos(k_x a) - \cos(k_y a)]$ are used for both figures. The other parameters are: (a) $t'/t = 0.16, t'' = 0, \Delta_0 = 6$ meV; (b) $t'/t = 0.2, t''/t = 0.25, \Delta_0 = 15$ meV.

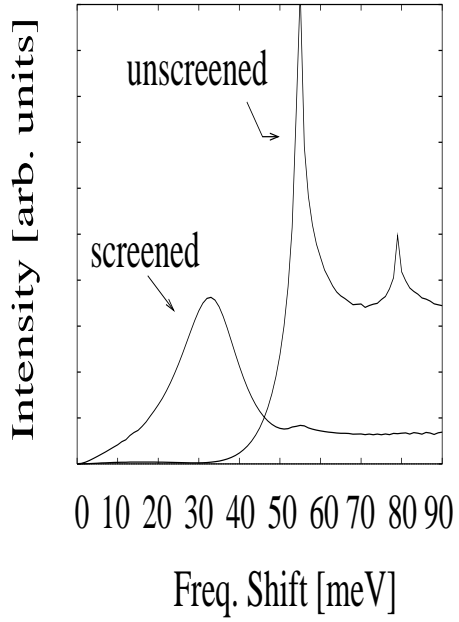


Figure 2: A_{1g} response calculated for a single band with and without Coulomb screening for the Y 1:2:3 parameters.

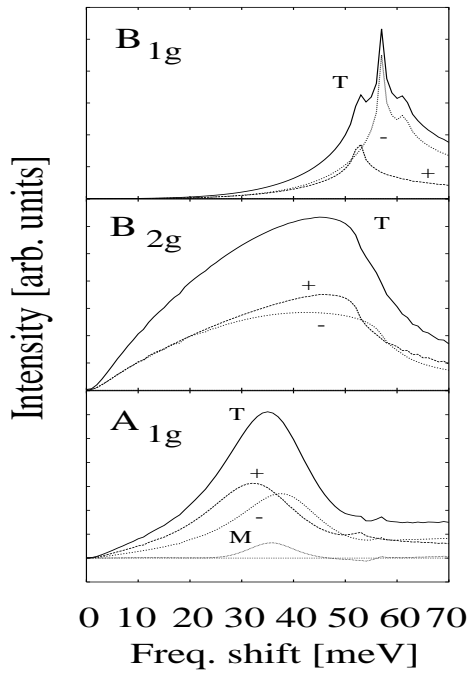


Figure 3: Raman response calculated for Y 1:2:3 bi-layer for various channels as indicated. The $+(-)$ indicates the bonding (anti-bonding) band, respectively, the symbol M is the mixing term [Eq. (14) which only contributes for the A_{1g} channel], and the total response is indicated by the symbol T .

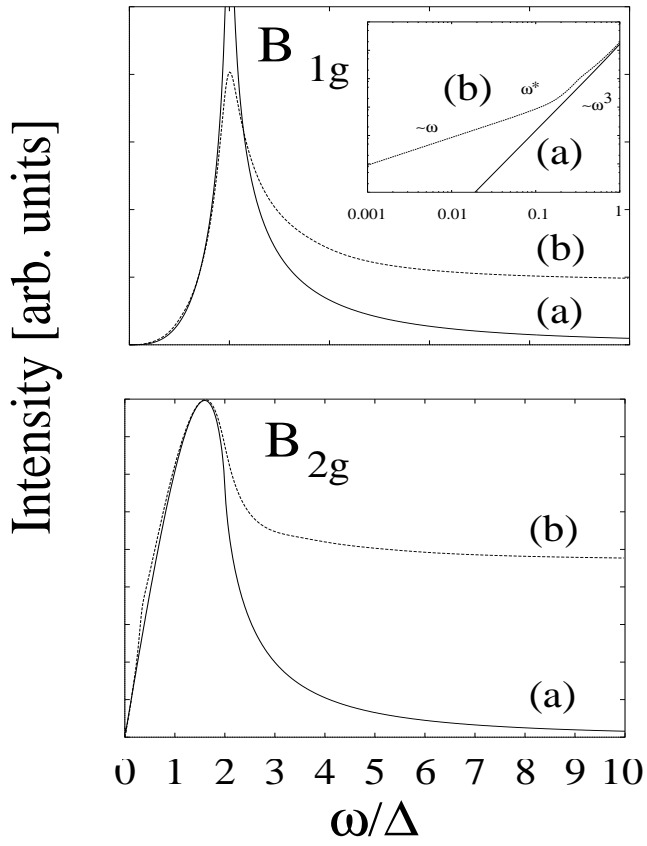


Figure 4: Raman response calculated for B_{1g} and B_{2g} channels in the absence (a) and presence (b) of impurity and spin fluctuation scattering. Inset shows the low frequency crossover of the B_{1g} channel. Parameters used are described in text.